ADVANCED FUNCTIONAL MATERIALS

Supporting Information

for *Adv. Funct. Mater.*, DOI: 10.1002/adfm.202002434

Pinecone-Inspired Nanoarchitectured Smart Microcages Enable Nano/Microparticle Drug Delivery

*Shichao Zhang, Sheng Zhou, Hui Liu, Malcolm Xing, Bin Ding, and Bingyun Li**

Supporting Information

Pinecone-Inspired Nanoarchitectured Smart Micro-Cages Enable Nano-/Microparticle Drug Delivery

*Shichao Zhang, Sheng Zhou, Hui Liu, Malcolm Xing, Bin Ding, and Bingyun Li**

Supporting Information

Pinecone-Inspired Nanoarchitectured Smart Micro-Cages Enable Nano-/Microparticle Drug Delivery

*Shichao Zhang, Sheng Zhou, Hui Liu, Malcolm Xing, Bin Ding, and Bingyun Li**

Dr. S. Zhang, Dr. S. Zhou, Prof. B. Li
Department of Orthopedics, School of Medicine, West Virginia University, Morgantown, WV, USA.
E-mail: bili@hsc.wvu.edu

Dr. H. Liu, Prof. B. Ding
Innovation Center for Textile Science and Technology, Donghua University, Shanghai, China

Prof. M. Xing
Department of Mechanical Engineering, University of Manitoba, and The Children's Hospital Research Institute of Manitoba, Winnipeg, MB, Canada.

Supporting Information contains:

Supplementary Figure S1-S15

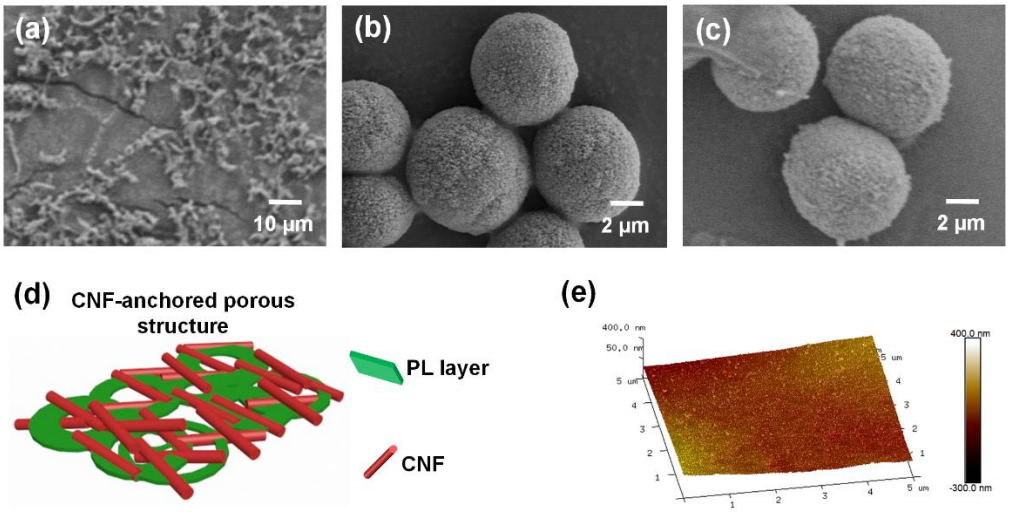

Figure S1. SEM images of (a) freeze-dried CNFs, (b) $CaCO_3$ microparticles, (d) PL/CNF_2 shelled $CaCO_3$ particles. (d) Schematic description of the assembly of CNFs and PL layer to form porous shell structures. (e) (h) AFM image of PL coated film on silicate wafer.

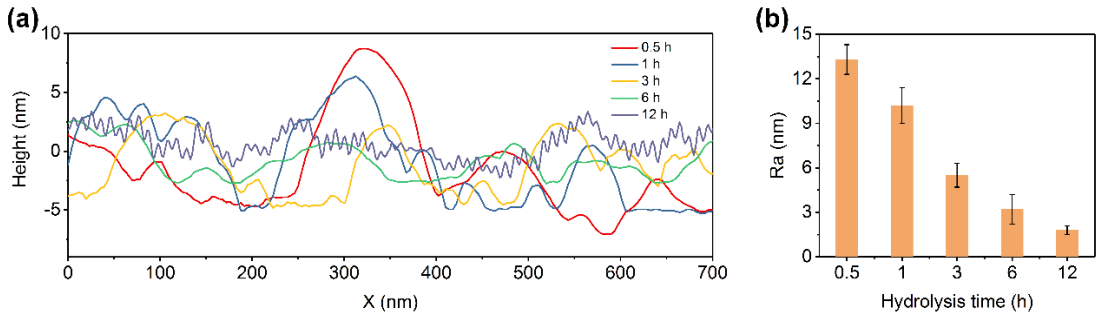

Figure S2. Surface roughness of (a) height along x-axis and (b) average Ra value of the films assembled using CNFs obtained under different hydrolysis time. In contrast to the roughness (Ra of 13.3) of CNF layer obtained with 0.5 h of hydrolysis, hydrolysis time of 12 h caused significantly reduced Ra of 1.8, due to dissociation.

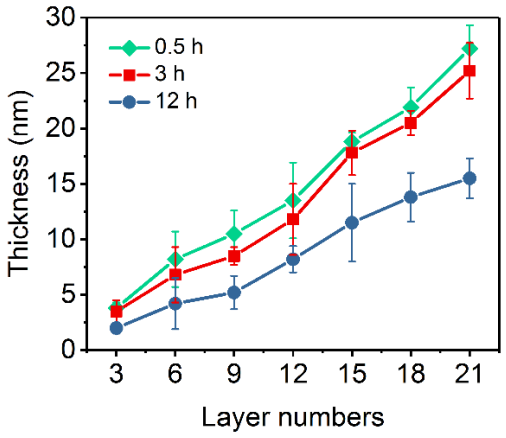

Figure S3. Growth profiles of CNF assembled nanofilms on silica templates at hydrolysis of 0.5, 3, and 12 h.

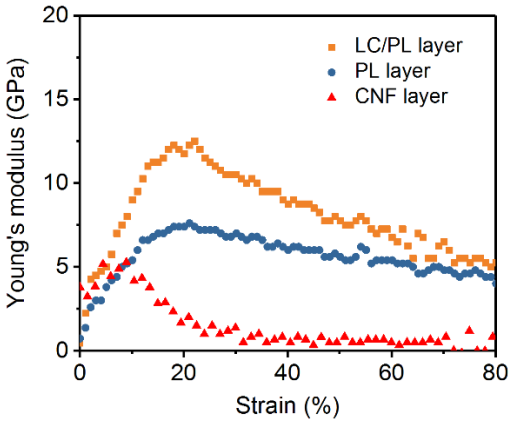

Figure S4. Young's modulus as a function of indentation strain of CNF, PL, and LC/PL films.

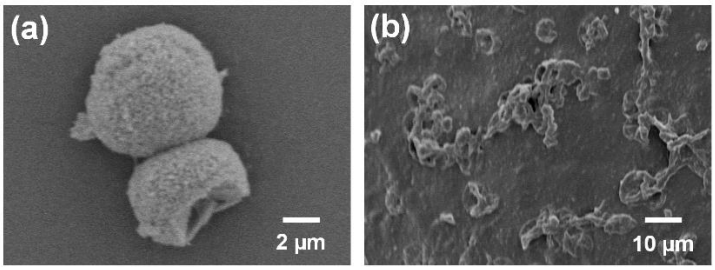

Figure S5. SEM images of (a) LC3 shelled $CaCO_3$ particles and (b) LC3 micro-cages on the PL coated substrates.

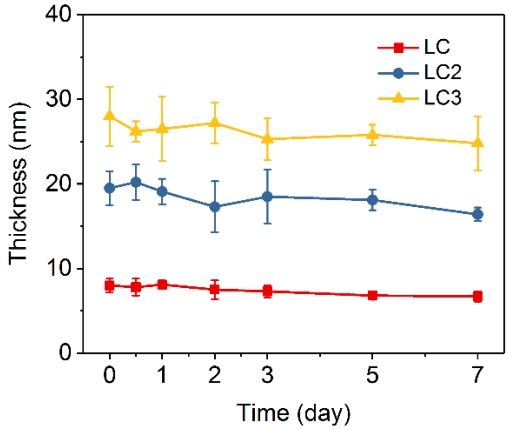

Figure S6. Thickness of the PL/CNF films after immersing in PBS for various times.

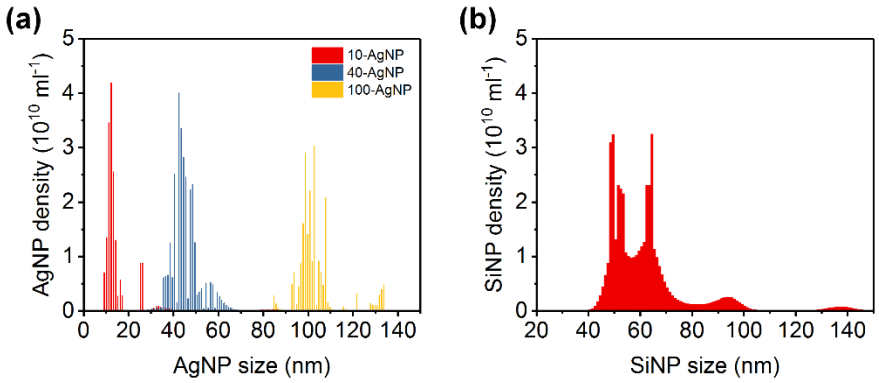

Figure S7. Size distribution of (a) AgNPs and (b) SiNPs studied.

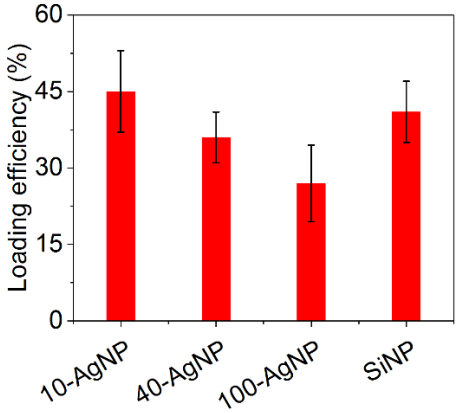

Figure S8. Loading efficiencies of AgNPs and SiNPs in the micro-cages.

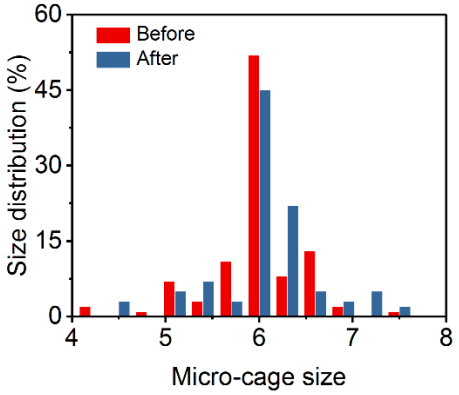

Figure S9. Size distribution of the micro-cages before and after drug loading.

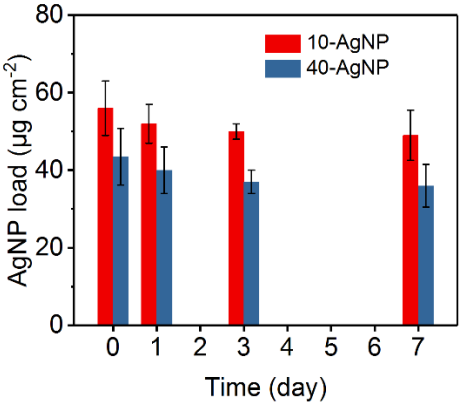

Figure S10. AgNP loading capability (drug-loading incubation time of 60 min) of LC3 micro-cages after storing the micro-cages in PBS for various times.

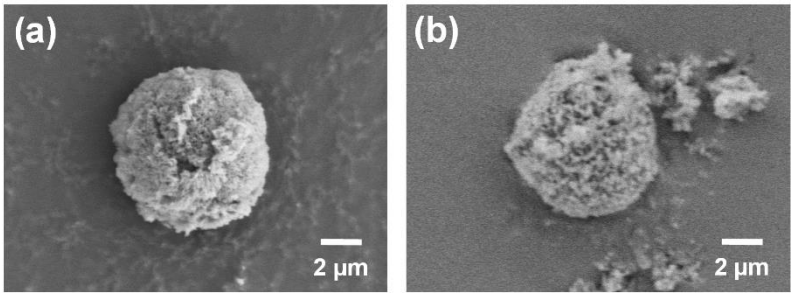

Figure S11. SEM images of the micro-cages after immersing in PBS of pH 4.0 for (a) 3 and (b) 7 days.

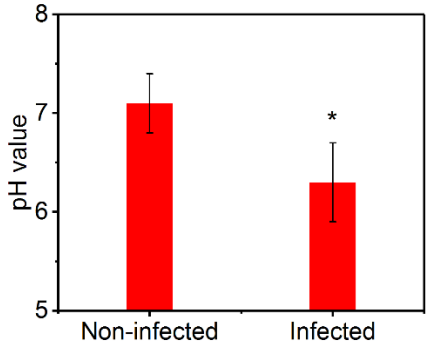

Figure S12. pH values of tissue samples around infected and uninfected rat femurs in our open fracture rat model. Using our previously reported open fracture rat model, we measured the pH of tissue samples around infected and uninfected femurs at post-operative day 10. *p <0.05 comparted to the uninfected samples.

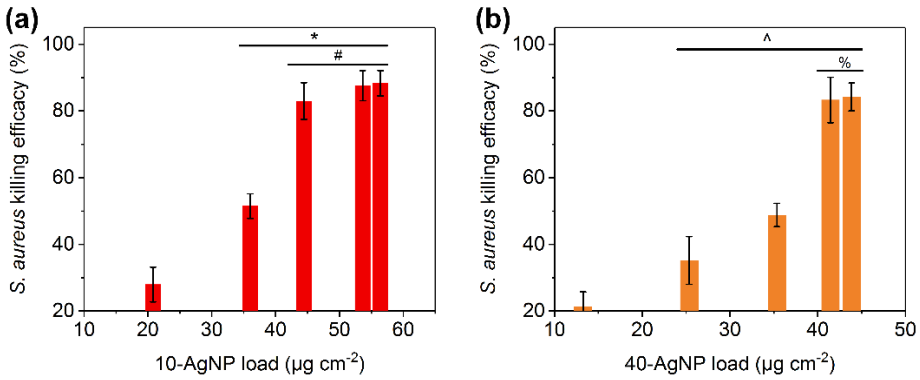

Figure S13. *S. aureus* killing efficacy of LC3 microcages loaded with different doses of (a) 10-AgNPs and (b) 40-AgNPs. *p < 0.01 compared to 23.2 μg cm^{-2}. #p < 0.05 compared to 38.4 μg cm^{-2}. ^p < 0.01 compared to 15.3 μg cm^{-2}. %p < 0.01 compared to 27.4 and 37.2 μg cm^{-2}.

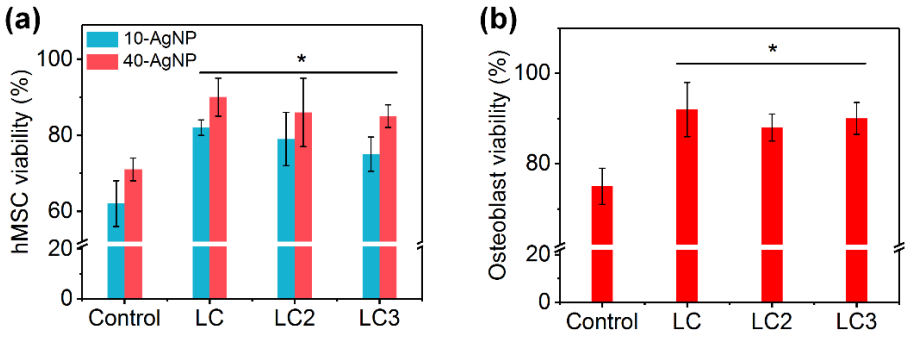

Figure S14. (a) hMSC viability on various micro-cage coated substrates with AgNP loading and the control (50 μM AgNP suspensions). (b) Osteoblast viability on the control substrate and substrates coated with micro-cages incorporated with SiNPs.

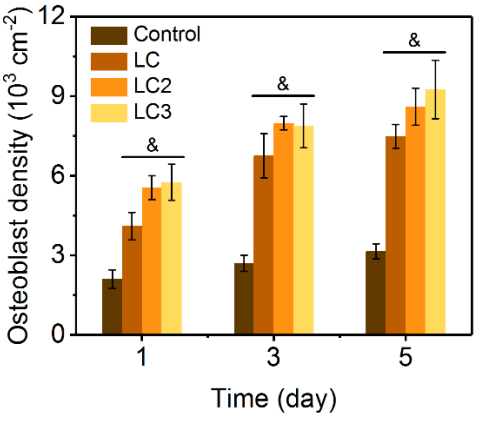

Figure S15. Proliferation of osteoblast cells on various substrates at 1, 3, and 5 days. &p < 0.01 compared to the controls.